Inorganic Chemistry

Article

pubs.acs.org/IC

Selective and Effective Stabilization of Mo^{VI}=O Bonds by NH···S Hydrogen Bonds via *Trans* Influence

Taka-aki Okamura,* Miki Tatsumi, Yui Omi, Hitoshi Yamamoto, and Kiyotaka Onitsuka

Department of Macromolecular Science, Graduate School of Science, Osaka University, Toyonaka, Osaka 560-0043, Japan

Supporting Information

ABSTRACT: A monooxomolybdenum(IV) complex containing two intramolecular NH···S hydrogen bonds, $(NEt_4)_2[Mo^{IV}O(1,2\text{-}S_2\text{-}3\text{-}t\text{-}BuNHCOC_6H_3)_2]$, was synthesized. The *trans* isomer was crystallized as the major product, and the molecular structure was determined by X-ray analysis. The *trans* isomer was isomerized by heating in solution to give a 1:1 mixture of *trans* and *cis* isomers. Oxidation of these isomers by Me_3NO afforded $(NEt_4)_2[Mo^{VI}O_2(1,2\text{-}S_2\text{-}3\text{-}t\text{-}BuNHCOC_6H_3)_2]$. ^1H NMR analysis revealed that the dioxomolybdenum(VI) complex existed as a single isomer where both oxo ligands were *trans* to each of the two hydrogen-bonded thiolate ligands. The Mo^{VI}=O bond was effectively stabilized by the NH···S hydrogen bond via *trans* influence, which was determined using resonance Raman spectroscopy. These results were supported by preliminary density functional theory calculations.

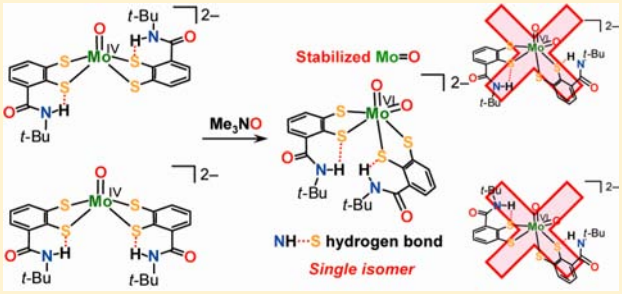

INTRODUCTION

Molybdenum enzymes are widely distributed in both eukaryotes and prokaryotes, and contain one or two unique pyranopterin dithiolene moieties called molybdopterin cofactors, with the exception of nitrogenase and few other proteins with unknown function.[1,2] Molybdopterin cofactors have been found exclusively in molybdenum and tungsten enzymes,[3,4] strongly suggesting that the dithiolene ligand is essential for the activity of these enzymes. The enzymes catalyze the oxidoreduction of various substrates in the redox cycle using Mo^{IV} and Mo^{VI} oxidation states. Molybdoenzymes are classified into three major families according to the number and kinds of ligands they contain.[3] The members of dimethyl sulfoxide (DMSO) reductase family possess two molybdopterin cofactors and an oxo ligand in the oxidized state. The reduced molybdenum(IV) center of DMSO reductase or trimethylamine *N*-oxide reductase reductively eliminates an oxygen atom from the substrate, DMSO or Me_3NO, respectively, resulting in the formation of a Mo^{VI}=O bond. The oxygen-atom-transfer reactions are thought to be the appropriate model reactions, and hence, numerous model complexes have been reported.[5−8]

In 1990, we found that the monooxomolybdenum(IV) benzenedithiolate complex, $(NEt_4)_2[Mo^{IV}O(bdt)_2]$ (bdt =1,2-benzenedithiolato), originally reported by Garner et al.,[9] catalyzed the biomimetic oxygen-atom-transfer reaction between amine *N*-oxide and benzoin to give amine, benzil, and water.[10] Moreover, the oxidized complex $(NEt_4)_2[Mo^{VI}O_2(bdt)_2]$ was isolated, and its molecular structure was successfully determined by X-ray analysis as the first such example of a dioxomolybdenum(VI) bis(dithiolate) complex.[11] The structure revealed that the Mo—S bond *trans* to the Mo=O bond was elongated due to the strong electron donation of the oxo ligand via *trans* influence; in addition, the S—C bond was shortened, suggesting a degree of thioketone (S=C) character,[11,12] which is closely related to the non-innocent behavior found in $[Mo^{VI}(bdt)_3]$.[13] In contrast, the Mo^{VI}=O bond was stabilized by the weak Mo—S bond at the *trans* position.

In our previous report, we demonstrated that the introduction of four NH···S hydrogen bonds into $[Mo^{IV}O(bdt)_2]^{2-}$ significantly accelerated the reduction of Me_3NO.[14] Unfortunately, the oxidized dioxomolybdenum(VI) complexes proved to be too unstable to be isolated. However, the corresponding dioxotungsten(VI) derivatives are fairly stable, and the analysis of isolated complexes indicated that the NH···S hydrogen bond stabilizes the W^{VI}=O bond at the *trans* position.[15] The crystal structure and IR spectra of $(NEt_4)_2[W^{VI}O_2\{1,2\text{-}S_2\text{-}3,6\text{-}(CH_3CONH)_2C_6H_2\}_2]$ demonstrated that the NH···S hydrogen bond at the *trans* position to the oxo ligand is significantly stronger than that at *cis* position. These facts suggest that the hydrogen bond at the *cis* position does not contribute to the stabilization of M=O but, on the contrary, destabilizes the oxidized state. This suggestive result inspired us to propose the presence of an intramolecular NH···S hydrogen bond in the pterin cofactor (Figure 1a).[14,15]

In this Article, we describe the introduction of an NH···S hydrogen bond unsymmetrically into a bdt ligand (Figure 1b) and the use of this ligand to synthesize monooxomolybdenum(IV) and dioxomolybdenum(VI) complexes with two intramolecular NH···S hydrogen bonds. Model studies using unsymmetrical ligands are limited due to synthetic difficulties;

Received: July 21, 2012
Published: October 17, 2012

dx.doi.org/10.1021/ic301597d | *Inorg. Chem.* 2012, 51, 11688−11697

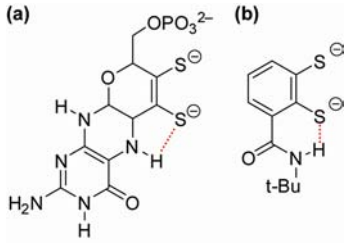

Figure 1. Proposed intramolecular NH···S hydrogen bond in a molybdopterin (a) and the model ligand (b).

however, both early[16,17] and recent[18,19] work using unsymmetrically heterocyclic substituted dithiolenes clearly indicate the contribution of the resonance form over dithiolene and the adjacent aromatic ring with unsymmetrical thione−thiolate electronic structure. Here, we discuss the formation of an unsymmetrical dithiolato ligand with an NH···S hydrogen bond, and the contributions of this hydrogen bond to the unsymmetrical electronic structures of model complexes using X-ray analysis, spectral measurements, and theoretical calculations.

EXPERIMENTAL SECTION

All procedures were performed under argon atmosphere by the Schlenk technique. All solvents were dried and distilled under argon before use.

Materials. 2,3-Dimercapto-1-benzoic acid,[20] $(NEt_4)[Mo^{V}O(SPh)_4]$,[21] and $(NEt_4)_2[Mo^{IV}O(S\text{-}4\text{-}ClC_6H_4)_4]$,[22] were prepared by the reported methods.

***N-tert*-Butyl-2,3-di(pivaloylthio)benzamide.** 2,3-Dimercapto-1-benzoic acid (2.87 g, 15 mmol) was dissolved in THF (160 mL). To the solution was added dropwise triethylamine (8.66 mL, 62 mmol) and pivaloyl chloride (6.26 mL, 51 mmol) cooling in an ice-salt bath. The obtained yellow suspension was allowed to warm up to room temperature, and stirring was continued overnight. The volatile materials were removed under reduced pressure, and THF (60 mL) was added to the residue. To the mixture was added dropwise *t*-butylamine (1.63 mL, 15 mmol), and the mixture was stirred overnight. The yellow suspension turned to blue. The blue suspension was concentrated *in vacuo*. To the residue was added water and ethyl acetate. The organic layer was separated, washed successively with 2% HCl aq, sat. NaCl aq, 4% $NaHCO_3$ aq, and sat. NaCl aq, and then dried over Na_2SO_4. The solution was concentrated under reduced pressure to give a green residual oil, which was recrystallized from hot ethyl acetate to give off-white powder. Yield 2.69 g (43%). ^{1}H NMR (dimethylsulfoxide-d_6): δ 1.23 (s, 9H), 1.24 (s, 9H), 1.32 (s, 9H), 7.42 (d, 1 H), 7.54 (t, 1H), 7.58 (d, 1H), 7.79 (s, 1H). Anal. Calcd for $C_{21}H_{31}NO_3S_2$: C, 61.58; H, 7.63; N, 3.42. Found: C, 61.49; H, 7.66; N, 3.42.

***N-tert*-Butyl-2,3-dimercaptobenzamide.** To a solution of *N-tert*-butyl-2,3-di(pivaloylthio)benzamide (312 mg, 0.76 mmol) in methanol (10 mL) was added dropwise 2 M NaOH aq (2.5 mL, 5.0 mmol) at 0 °C. The reaction mixture was stirred overnight at 25 °C to give a yellow solution. The solution was concentrated under reduced pressure to dryness. To the residue was added water and acidified with 2% HCl aq. The separated product was extracted with ethyl acetate. The organic layers were combined and washed with water and sat. NaCl aq, and then dried over Na_2SO_4. Removal of the solvent under reduced pressure gave off-white solid, which was recrystallized from diethyl ether to give colorless needles. Yield 63.5 mg (35%). ^{1}H NMR ($CDCl_3$): δ 7.39 (dd, J = 7.8, 1.4 Hz, 1H, Ar), 7.18 (dd, J = 7.6, 1.4 Hz, 1H, Ar), 7.02 (t, J = 7.7 Hz, 1H, Ar), 5.71 (br, 1H, NH), 5.40 (s, 1H, SH), 3.77 (s, 1H, SH), 1.47 (s, 9H, *t*-Bu). Anal. Calcd for $C_{11}H_{15}NOS_2$: C, 54.74; H, 6.26; N, 5.80. Found: C, 54.28; H, 6.17; N, 5.74.

$(NEt_4)_2[Mo^{IV}O(1,2\text{-}S_2\text{-}3\text{-}t\text{-}BuNHCOC_6H_3)_2]$ (1). The complex was synthesized by a ligand exchange reaction using the dithiolate ligand or thioester.

Method 1. A mixture of $(NEt_4)[Mo^{V}O(SPh)_4]$ (99 mg, 0.15 mmol) and *N-tert*-butyl-2,3-di(pivaloylthio)benzamide (120 mg, 0.29 mmol) in 1,2-dimethoxyethane (DME) (5 mL) was stirred at 60 °C for 6 days. The precipitate was collected by centrifugal separation and washed with DME and diethyl ether. When the precipitate contains molybdenum(V) species, a gray precipitate was deposited; however, the reduction by NEt_4BH_4 in acetonitrile was effective to give a clear yellow precipitate. The yellow precipitate was recrystallized from acetonitrile/diethyl ether to afford orange blocks. Yield 5 mg (4%). The spectral data were identical with those of the product synthesized by the following method.

Method 2. A solution of *N-tert*-butyl-2,3-dimercaptobenzamide (49.2 mg, 0.204 mmol) in DME (1.5 mL) was added dropwise to a solution of $(NEt_4)_2[Mo^{IV}O(S\text{-}4\text{-}ClC_6H_4)_4]$ (91.2 mg, 0.096 mmol) in acetonitorile (1 mL) to give a green solution. The mixture was stirred for 3 h to give a reddish brown solution, and concentrated to dryness under reduced pressure. The residue was washed with DME several times to give a yellow powder. Recrystallization from acetonitorile gave orange microcrystals, which were washed with diethyl ether (1 mL × 2) and dried under reduced pressure. Yield 28.8 mg (35.3%). ^{1}H NMR (303 K, CD_3CN): δ 9.14 (s, 1H, NH), 7.68 (d, J = 6.2 Hz, 1H, Ar), 7.48 (d, J = 7.3 Hz, 1H, Ar), 6.83 (t, J = 7.4 Hz, 1H, Ar), 2.97 (q, J = 7.3 Hz, 8H, $CH_2(NEt_4)$), 1.54 (s, 9H, *t*-Bu), 1.06 (tt, J = 7.3, 1.9 Hz, 12H, $CH_3(NEt_4)$). Anal. Calcd for $C_{38}H_{66}N_4O_3S_4Mo\cdot H_2O$: C, 52.51; H, 7.89; N, 6.45. Found: C, 52.58; H, 7.77, N, 6.47.

$(NEt_4)_2[Mo^{VI}O_2(1,2\text{-}S_2\text{-}3\text{-}t\text{-}BuNHCOC_6H_3)_2]$ (2). To a DMF solution (0.51 mL) of **1** (1.67 mg, 1.9 μmol) was added 50 μL of DMF solution containing 0.29 mg (3.9 μmol) of trimethylamine *N*-oxide at room temperature. The pale yellow solution turned immediately red. The solution was concentrated to dryness under reduced pressure. The product was used for the spectral measurements without further purification. ^{1}H NMR spectra revealed that the oxidation proceeded quantitatively to afford pure **2** as described in the Results section.

Physical Measurements. UV−vis absorption spectra were recorded using a SHIMADZU UV-3100PC spectrometer. Infrared (IR) spectroscopic measurements in the solid state were done on a Jasco FT/IR-8300 spectrometer. Samples were prepared as KBr disks and CH_2Cl_2 solution (2 mM). ^{1}H NMR spectra were obtained with a Jeol LA-500 spectrometer in dimethylsulfoxide-d_6, dichloromethane-d_2, or acetonitrile-d_3 at 30 °C. Nuclear Overhauser effect (NOE) correlated spectroscopy (NOESY), heteronuclear single quantum coherence (HSQC), gradient enhanced NOE spectroscopy (GOESY), and heteronuclear multiple bond connectivity (HMBC) spectra were recorded on a Varian UNITYplus 600 MHz at −10 °C. Electrospray ionization mass spectroscopy (ESI-MS) measurements were performed on a Finnigan MAT LCQ ion trap mass spectrometer in a acetonitrile solution. The measurements of cyclic voltamograms in DMF solusion were carried out on a BAS 100B/W instrument with a three-electrode system: glassy carbon working electrode, a Pt-wire auxiliary electrode, and reference electrode. The scan rate was 100 mV/s. Concentration of sample was 2 mM, containing 0.1 M of *n*-Bu_4NClO_4 as a supporting electrolyte. Potentials were determined at room temperature versus saturated calomel electrode (SCE) or Ag/$AgNO_3$ (10 mM in acetonitrile) as a reference. In the case of SCE, values uncorrected for junction potential were obtained. In the same condition, ferrocene/ferrocenium redox couple was observed at +0.48 V versus SCE. Although the junction potential presumably depends on the conditions of the interface, the reproducibility within 0.01 V was observed. The data were consistent with the values versus Ag/$AgNO_3$. In the present condition, ferrocene/ferrocenium redox couple was observed at +0.28 V versus Ag/$AgNO_3$. Raman spectra were measured at 298 K on a Jasco NR-1800 with liq N_2 cooled CCD detector. Exciting radiation was provided by Ar^+ ion (514.5 nm).

Kinetic Measurements. Reaction systems containing the monooxomolybdenum(IV) complex and Me_3NO were monitored spectorometrically in the region 250−700 nm. A typical measurement

dx.doi.org/10.1021/ic301597d | Inorg. Chem. 2012, 51, 11688−11697

Scheme 1. Synthetic Route for Monooxomolybdenum(IV) Complex

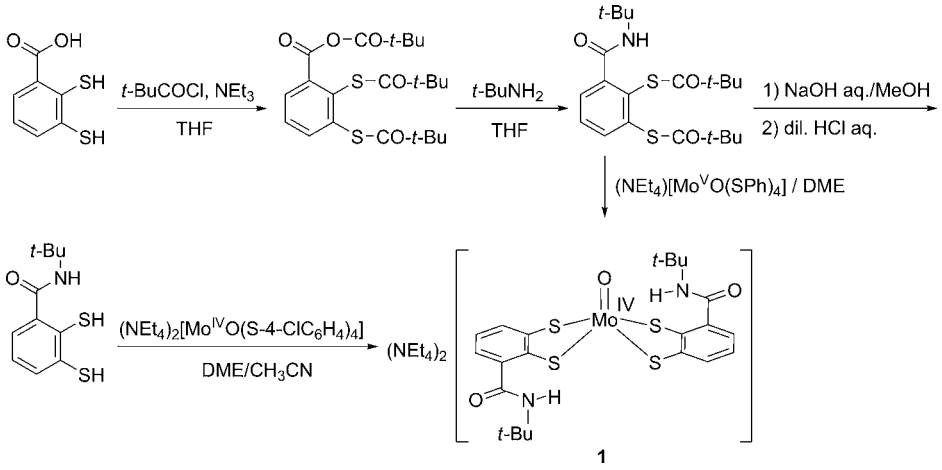

was carried out using a 1-mm UV cell containing a solution of monooxomolybdenum(IV) complex **1** (1 mM, 0.3 mL) at 27 °C. After thermal equilibrium, a Me_3NO solution (60 mM, 10 μL, also at 27 °C) was injected through a silicone rubber cap, and the cell contents were quickly mixed by shaking. The time dependence of the absorbance for dioxomolybdenum(VI) was measured. All calculations for the data analysis were performed using the absorbance at 506 nm (O and S → Mo^{VI} charge transfer band).

X-ray Structure and Determination. Each single crystal of **1** and *N-tert*-butyl-2,3-di(pivaloylthio)benzamide was selected carefully and mounted in a loop with Nujol, which was frozen immediately in a stream of cold nitrogen at 200 K. Data collection was made on a Rigaku RAXIS-RAPID Imaging Plate diffractometer with graphite monochromated Mo Kα radiation (0.710 75 Å). The structures were solved by SIR92[23] and expanded by Fourier technique using SHELXL-97.[24] All non-hydrogen atoms were refined anisotropically. All hydrogen atoms were placed at the calculated positions using the riding model.

Theoretical Calculations. Geometry optimizations and natural bond order (NBO) analysis were performed at the density functional theory (DFT) level using Becke's three parameter hybrid functionals (B3LYP) in Gaussian 03[25] program package. The basis set used for Mo was MINI-1[26] supplemented by the 5p AO with the same exponent as that for the 5s AO.[27] For the other atoms (H, C, N, O, F, S), 6-31G** basis set was employed. The coordinates of the crystal structures, $(NEt_4)_2[MoO(S_2\text{-}3\text{-}t\text{-}BuNHCOC_6H_3)_2]$ (**1**), $(NEt_4)_2[MoO\{1,2\text{-}S_2\text{-}3,6\text{-}(CH_3CONH)_2C_6H_2\}_2]$,[14] and $(NEt_4)_2[WO_2\{1,2\text{-}S_2\text{-}3,6\text{-}(CH_3CONH)_2C_6H_2\}_2]$[15] were used for the initial structures with some modifications.

RESULTS

Synthesis. A precursor of the dithiolato ligand, *N-tert*-butyl-2,3-di(pivaloylthio)benzamide, was synthesized using a traditional mixed anhydride method,[28] as shown in Scheme 1. The thioester was fully characterized by ^1H NMR, X-ray analysis, and elemental analysis. The results of X-ray analysis are given in the Supporting Information. The two thioester moieties and an amide group were approximately perpendicular to the benzene ring and formed intermolecular NH···O=C hydrogen bonds in a dimeric structure (Figure S1). The thioester reacted slowly with $(NEt_4)[Mo^VO(SPh)_4]$ in 1,2-dimethoxyethane (DME) accompanying the autoreduction of Mo(V) to Mo(IV) to afford $(NEt_4)_2[Mo^{IV}O(1,2\text{-}S_2\text{-}3\text{-}t\text{-}BuNHCOC_6H_3)_2]$ (**1**) in a low yield. The reaction most likely proceeded via a thioester exchange reaction following autoreduction. Preliminary experiments using $(NEt_4)_2[Ni^{II}(SPh)_4]$[29] revealed that thioester exchange occurred, and the resulting *t*-BuCOSPh was detected by ^1H NMR spectra. When the crude product was contaminated with a molybdenum(V) species, reduction using a small amount of NEt_4BH_4 was effective for obtaining a pure product. An alternative to the reported procedure[30] is here. Dithiol was prepared by hydrolysis of the thioester and allowed to react with $(NEt_4)_2[Mo^{IV}O(S\text{-}4\text{-}ClC_6H_4)_4]$[22] to give **1** in a reasonable yield. ^1H NMR spectra of the microcrystalline product revealed predominantly the *trans* isomer with a *trans*/*cis* ratio of about 4:1, which suggests that the formation of the *trans* isomer is kinetically favorable. The structural assignments are described in the following section. A similar preferential formation or crystallization of one isomer over the other was found previously in a similar case using unsymmetrical ligands.[17]

The monooxomolybdenum(IV) complex **1** readily reacted with Me_3NO to afford the dioxomolybdenum(VI) complex, $(NEt_4)_2[Mo^{VI}O_2(1,2\text{-}S_2\text{-}3\text{-}t\text{-}BuNHCOC_6H_3)_2]$ (**2**), which was relatively stable in comparison with $(NEt_4)_2[Mo^{VI}O_2(bdt)_2]$ (**6**)[11,12] and $(NEt_4)_2[Mo^{VI}O_2\{1,2\text{-}S_2\text{-}3,6\text{-}(CH_3CONH)_2C_6H_2\}_2]$.[14] Compound **2** was isolated as a solid and exhibited sufficient stability for spectral analysis. The solid was dissolved in acetonitrile and analyzed using ESI-MS. In a negative mode, anionic $[(NEt_4)[Mo^{VI}O_2(1,2\text{-}S_2\text{-}3\text{-}t\text{-}BuNHCOC_6H_3)_2]]^-$ (calcd m/z 738.1) and $[Mo^{VI}O_2(1,2\text{-}S_2\text{-}3\text{-}t\text{-}BuNHCOC_6H_3)_2]^{2-}$ (calcd m/z 304.0) were detected, and the characteristic isotope patterns were in agreement with simulations. Some intense fragment peaks were observed, which were probably caused by the decay of the parent ions in the ionization process. All major peaks were assignable to reasonable fragment ions (Figure S2). The molybdenum(VI) center was sometimes electrically reduced to molybdenum(V) in the ion source.

Molecular Structure in the Crystal. The crystal structure of **1** is shown in Figure 2. Complex **1** has essentially square-pyramidal geometry, and thus both *trans* and *cis* configurations are possible, as illustrated in Chart 1. Only one isomer, *trans*-**1**, was crystallized selectively. Selected geometrical parameters are listed in Table 1 with the related compounds, $(NEt_4)_2[Mo^{IV}O(bdt)_2]$ (**3**), which lacks hydrogen bonds, and $(NEt_4)_2[Mo^{IV}O\{1,2\text{-}S_2\text{-}3,6\text{-}(CH_3CONH)_2C_6H_2\}_2]$ (**4**), which contains four intramolecular NH···S hydrogen bonds. Amide NH groups of **1** are directed toward the neighboring thiolate sulfur atom, potentially forming intramolecular NH···S hydrogen bonds, where N1···S12 and N2···S22 are 3.016(7) and 3.006(7) Å,

dx.doi.org/10.1021/ic301597d | Inorg. Chem. 2012, 51, 11688−11697

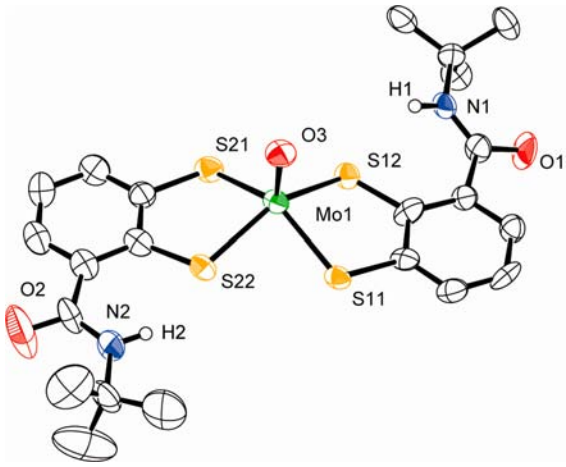

Figure 2. Molecular structure of the anion part of $(NEt_4)_2[Mo^{IV}O(1,2\text{-}S_2\text{-}3\text{-}t\text{-}BuNHCOC_6H_3)_2]$ (**1**).

Chart 1. Two Isomers of 1

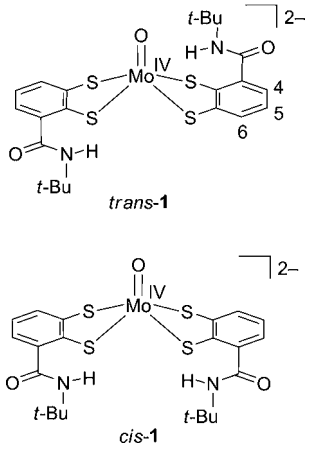

Table 1. Selected Bond Distances (Å) for the Anions of $(NEt_4)_2[Mo^{IV}O(1,2\text{-}S_2\text{-}3\text{-}t\text{-}BuNHCOC_6H_3)_2]$ (1), $(NEt_4)_2[Mo^{IV}O(bdt)_2]$ (3), and $(NEt_4)_2[Mo^{IV}O\{1,2\text{-}S_2\text{-}3,6\text{-}(CH_3CONH)_2C_6H_2\}_2]$ (4)

	1	3[a]	4[b]
Mo=O	1.698(6)	1.699(6)	1.672(4)
Mo—S (mean)	2.369(17)	2.388(2)	2.386(6)
Mo—S11	2.348(2)	2.391(2)	2.383(2)
Mo—S12	2.385(2)	2.384(2)	2.377(2)
Δ(Mo—S)[c]	0.037	0.007	0.006
Mo—S21	2.356(2)	2.391(2)	2.393(2)
Mo—S22	2.385(2)	2.384(2)	2.389(2)
Δ(Mo—S)[c]	0.029	0.007	0.004

[a]Two anions I and II are present, and the dimensions are not significantly different from each other. Here is shown the data for anion I (ref 9). [b]Reference 14. [c]Δ(Mo—S) = |(Mo—S11) − (Mo—S12)| or |(Mo—S21) − (Mo—S22)|.

respectively. Estimated geometry using fixed N—H distance (0.88 Å) indicated preferable distances and angles, H1···S12 (2.36 Å), H2···S22 (2.22 Å), N1—H1···S12 (132°), and N2—H2···S22 (149°), for the formation of NH···S hydrogen bonds. The presence of the unsymmetrical ligand resulted in an unsymmetrical coordination environment. The two Mo—S bonds are distinguishable from each other, and the mean length of the Mo—S bond is shorter than that of **3**. The Mo—S12 and Mo—S22 bonds are significantly longer than the others in **1**, suggesting that the NH···S hydrogen bond electrostatically or covalently stabilizes the thiolate anion, causing the decrease in electron-donation from S to Mo.

Solution Structure of 1. The configuration of *trans*-**1** was sufficiently stable in solution at room temperature for spectroscopic analysis. When crystals of **1** were dissolved in acetonitrile-d_3, only one isomer, assumed to be *trans*-**1**, was observed in ^{1}H NMR spectra (Figure 3a). Next the solution

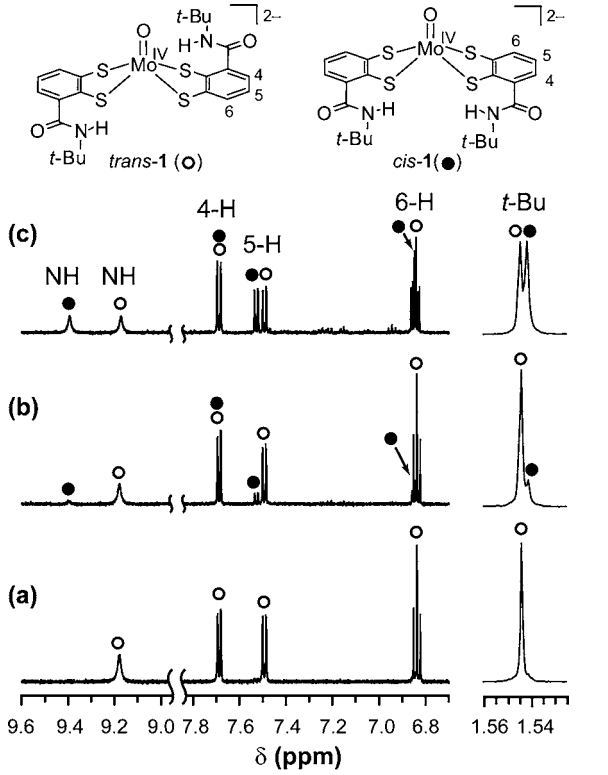

Figure 3. ^{1}H NMR spectra of $(NEt_4)_2[Mo^{IV}O(1,2\text{-}S_2\text{-}3\text{-}t\text{-}BuNHCOC_6H_3)_2]$ (**1**) in acetonitrile-d_6 at 30 °C: (a) *trans*-**1** isolated as crystals, (b) heated at 50 °C for 1 h, and (c) heated at 50 °C for 3 h. The *trans* isomer was isomerized gradually by heating to *cis*-**1**, and *trans*/*cis* ratio converged to 1:1. The set of chemical shifts for the *trans*/*cis* isomers are 9.17/9.39 (NH), 7.69 (4-H), 7.49/7.53 (6-H), 6.84/6.85 (5-H), and 1.541/1.538 (*t*-Bu).

was heated to 50 °C, and the conversion was monitored by ^{1}H NMR at 30 °C. Upon heating, *trans*-**1** gradually isomerized to *cis*-**1**, which was detected as distinct peaks. After 1 h, the *trans*/*cis* ratio was 6:1 (Figure 3b) and converged to 1:1 within 3 h (Figure 3c). These results demonstrated that the thermodynamic stabilities of the two isomers were identical.

^{1}H NMR spectra of *trans*-**1** in dichloromethane-d_2 exhibited an NH peak at 8.98 ppm at 30 °C. In contrast, the NH peak of *N*-*tert*-butyl-2,3-di(pivaloylthio)benzamide without intramolecular NH···S hydrogen bonds appeared at 5.68 ppm under the same conditions. The downfield shift of ~3.3 ppm strongly suggests the presence of tight NH···S hydrogen bonds in **1** that maintain their conformation in the crystal although the effects caused by the coordination of a molybdenum ion should be considered.

IR and Raman Spectra. The presence and the strength of the NH···S hydrogen bonds were established and evaluated

dx.doi.org/10.1021/ic301597d | *Inorg. Chem.* 2012, 51, 11688−11697

using IR spectra. The data relating to the amide NH and C=O stretching bands of **1** and **2** are listed in Table 2. Evaluation of

Table 2. IR Data of $(NEt_4)_2[Mo^{IV}O(1,2\text{-}S_2\text{-}3\text{-}t\text{-}BuNHCOC_6H_3)_2]$ (1) and $(NEt_4)_2[Mo^{VI}O_2(1,2\text{-}S_2\text{-}3\text{-}t\text{-}BuNHCOC_6H_3)_2]$ (2)

		ν(NH)[a]	$\Delta\nu$(NH)[d]	ν(C=O)[a]	$\Delta\nu$(C=O)
1	solid state[b]	3231	−198	1643	−16
	in CH_2Cl_2	3247	−182	1634	−25
2	solid state[c]	3220	−209	1641	−18

[a]In cm^{-1}. [b]In KBr disk. [c]In Nujol mull. [d]Difference from the values for the free amide group of $(S\text{-}2\text{-}t\text{-}BuNHCOC_6H_4)_2$ in CH_2Cl_2 (ref 31).

hydrogen bonds was performed utilizing a reported method using the values of the so-called free amide group without a hydrogen bond.[31] The values of $\Delta\nu$(NH) and $\Delta\nu$(C=O) are the differences from the free ν(NH) and ν(C=O) of $(S\text{-}2\text{-}t\text{-}BuNHCOC_6H_4)_2$, which lacks hydrogen bonds in CH_2Cl_2. The large negative values of $\Delta\nu$(NH) clearly indicate the presence of intramolecular NH···S hydrogen bonds in both the solid state and in solution. These results agree with the observations made using ^{1}H NMR spectra discussed above. The lower wavenumber of ν(NH) of **2** suggests the presence of a stronger NH···S hydrogen bond in comparison with that of **1**. The relatively small $\Delta\nu$(C=O) was caused by an inductive effect of the NH···S hydrogen bond and indicated the absence of an NH···O=C hydrogen bond, which was found in the other complexes.[31−33]

The data regarding Mo=O stretching of **1** in IR and resonance Raman spectra are listed in Table 3 along with values

Table 3. Spectroscopic Data and Redox Potentials of $(NEt_4)_2[Mo^{IV}O(1,2\text{-}S_2\text{-}3\text{-}t\text{-}BuNHCOC_6H_3)_2]$ (1), $(NEt_4)_2[Mo^{IV}O(bdt)_2]$ (3), $(NEt_4)_2[Mo^{IV}O\{1,2\text{-}S_2\text{-}3,6\text{-}(CH_3CONH)_2C_6H_2\}_2]$ (4), and $(NEt_4)_2[Mo^{IV}O(bdtCl_2)_2]$ (5)

		ν(Mo=O) /cm^{-1}		$E_{1/2}$[d]/V	
	λ_{max} nm (ε, M^{-1} cm^{-1})	Raman	IR	vs SCE	vs Ag/$AgNO_3$[e]
1	281 (35 000), 358 (10 800), 440 (890)	918	918	−0.26	−0.44
3[a]	328 (12 000), 385 (980), 452 (420)	902	905	−0.38	−0.58
4[b]	333 (5100), 380 (650), 452 (420)	921	922	−0.13	
5[c]	330 (9500), 394 (950)		910	−0.10	

[a]Referenes 9 and 30. [b]Reference 14. [c]Reference 36. [d]In DMF. [e]In acetonitrile.

for the related compounds. Complex **1** exhibited higher ν(Mo=O) than $(NEt_4)_2[Mo^{IV}O(bdt)_2]$ (**3**), which lacks NH···S hydrogen bonds, and was slightly lower than that of $(NEt_4)_2[Mo^{IV}O\{1,2\text{-}S_2\text{-}3,6\text{-}(CH_3CONH)_2C_6H_2\}_2]$ (**4**), which contains four intramolecular NH···S hydrogen bonds. These results suggest that the NH···S hydrogen bond decreases the electron donation from S to Mo and electron density on Mo, resulting in increased donation from O to Mo. A similar tendency was found in $(NEt_4)_2[Mo^{IV}O(bdtCl_2)_2]$ (**5**) with electron-withdrawing substituent groups (Cl). The trend is reasonable, but the relationship to the number and strength of hydrogen bonds could not be strictly described. This ambiguity is probably associated with distortion of the $MoOS_4$ local structure.[34]

The resonance Raman spectrum of **2** in the solid state is shown in Figure S3. Characteristic symmetric and asymmetric vibration modes of the MoO_2 moiety were observed as described in a previous report.[12,35] The ν_s(Mo=O) and ν_{as}(Mo=O) values are listed with the related compounds, $(NEt_4)_2[Mo^{VI}O_2(bdt)_2]$ (**6**),[12] which does not have substituents, and $(NEt_4)_2[Mo^{VI}O_2(bdtCl_2)_2]$,[36] which contains electron-withdrawing groups (Table 4). The values of **2** are higher

Table 4. Raman Bands (cm^{-1}) of $(NEt_4)_2[Mo^{VIO2}(1,2\text{-}S_2\text{-}3\text{-}t\text{-}BuNHCOC_6H_3)_2]$ (2) and the Related Complexes

	ν_s(Mo=O)	ν_{as}(Mo=O)
2	871	840
$(NEt_4)_2[Mo^{VI}O_2(bdt)_2]$ (**6**)[a]	858	829
$(NEt_4)_2[Mo^{VI}O_2(bdtCl_2)_2]$[b]	867 (868)	(839)

[a]Data from ref 12. [b]Reference 36. IR data are shown in the parentheses.

than those of the other compound, suggesting that the NH···S hydrogen bonds efficiently stabilized the Mo=O bonds as reported for analogous dioxotungsten(VI) complexes.[15]

Electrochemical Properties. The cyclic voltammogram of **1** exhibited pseudoreversible Mo(V)/Mo(IV) redox couple at $E_{1/2}$ = −0.26 V versus SCE, as shown in Figure S4. The redox potential is listed in Table 3 along with those of **3**−**5**. The value of **1** with two NH···S hydrogen bonds is more positive by 0.12 V than that of **3**, which lacks hydrogen bonds. Conversely, the measured redox potential for **4** with four NH···S hydrogen bonds was −0.13 V, which is +0.25 V (approximately twice as large as 0.12 V) in comparison with the redox potential of **3**. A similar simple correlation between the number of NH···S bonds and a positive shift in redox potential was identified previously for another series of complexes.[32,33,37] Direct electron-withdrawing groups can effectively induce a positive shift in redox potential, as observed for **5**.[36]

Absorption Spectra. The UV−vis spectrum of **1** is shown as an initial curve in Figure 4, and absorption maxima of **1** and **3**−**5** are summarized in Table 3. The spectra of **3**−**5** resemble each other, but **1** shows an intense peak at 358 nm. This maximum peak persisted during the oxidation to **2**, and thus most likely arises from absorption of the dithiolato ligand. Because the absorption peak at ∼300 nm observed for **3**−**5** is

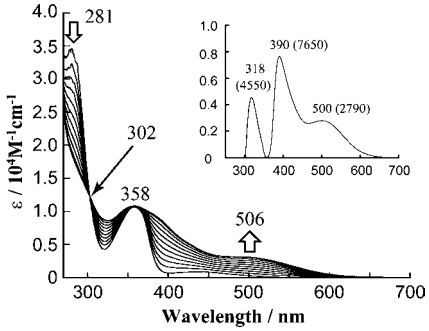

Figure 4. UV−vis spectral change (every 4 min) in the stoichiometric reduction of Me_3NO by **1** in DMF ($[Mo^{IV}]$ = 1 mM, $[Me_3NO]$ = 2 mM) at 27 °C. The spectra show spectral change from **1** to **2**. Inset shows difference of the absorption between $(NEt_4)_2[Mo^{VI}O_2(1,2\text{-}S_2\text{-}3\text{-}t\text{-}BuNHCOC_6H_3)_2]$ (**2**) and **1**.

dx.doi.org/10.1021/ic301597d | Inorg. Chem. 2012, 51, 11688−11697

assignable to the ligand-to-metal charge-transfer absorption (LMCT) band,[14] the LMCT band of **1** presumably overlapped in the shoulder of the intense peak in this region.

Reduction of Trimethylamine *N*-Oxide. The O atom transfer reduction of Me_3NO by **1** was monitored by UV−vis spectroscopy. A series of spectra taken every 4 min is shown in Figure 4, where [Mo] = 1 mM and [Me_3NO] = 2 mM in DMF at 27 °C. During the reaction, absorption at 281 nm decreased, and the absorption maximum at 506 nm increased slowly, showing isosbestic points at 302 and 358 nm. The reaction was virtually completed within ∼40 min. To exclude the intense absorption of the ligand, the difference of the absorption between **2** and **1** is shown in the inset of Figure 4. The maxima at 390 and 500 nm are assignable to LMCT bands, which are close to the reported values of 389 and 531 nm for $(NEt_4)_2[Mo^{VI}O_2\{1,2\text{-}S_2\text{-}3,6\text{-}(CH_3CONH)_2C_6H_2\}_2]$.[14]

The reaction was monitored at 506 nm and analyzed using pseudo-first-order kinetics at the initial stage. The observed rate constant was $k_{obs} = (9.6 \pm 1.0) \times 10^{-4}$ s^{-1} for 2 equiv of Me_3NO. When 10 equiv of Me_3NO ([Me_3NO] = 10 mM) was used, $k_{obs} = (37 \pm 6) \times 10^{-4}$ s^{-1}. The reaction obeyed second-order kinetics, and the obtained rate constants were $k_2 = (6.1 \pm 0.8) \times 10^{-1}$ M^{-1}s^{-1} for 2 equiv of Me_3NO and $k_2 = (4.4 \pm 0.5) \times 10^{-1}$ M^{-1} s^{-1} for 10 equiv. Under similar conditions, the observed rate constants for **3** and **4** with 2 equiv of Me_3NO were found to be $k_{obs} = (5.4 \pm 0.1) \times 10^{-4}$ s^{-1} and $k_{obs} = (49 \pm 1) \times 10^{-4}$ s^{-1}, respectively.[14] Compound **1**, containing two NH···S hydrogen bonds, exhibited a rate constant approximately twice that of **3**. While the presence of NH···S hydrogen bonds probably accelerated the reduction of Me_3NO by a similar mechanism as that described previously for **4**, which contains four NH···S hydrogen bonds,[14] the contribution per hydrogen bond is small. The difference is presumably caused by the difference in the two substituent groups, carbamoyl (RNHCO) and acylamino (RCONH). The former prefers to form six-membered NH···S hydrogen bonds but retains flexibility,[31] and the latter forms five-membered rings in rigid or fixed conformations. In the solid state or in less polar solvents, e.g., CH_2Cl_2, **1** formed strong NH···S hydrogen bonds as established by IR and ^{1}H NMR. However, in DMF, the amide groups were solvated, and NH groups interacted with carbonyls of DMF, resulting in weak hydrogen bonds and insufficient contributions to the reaction. Because of the solubility limits of Me_3NO and instability of the product **2** in CH_2Cl_2, the reaction could not be carried out in less polar solvents.

The stoichiometric reaction between a monooxomolybdenum(IV) complex and Me_3NO is following essentially second-order kinetics. In the case of complex **4**, saturation kinetics were shown in the range 6 mM ≤ [Me_3NO] ≤ 10 mM.[14] Similar kinetic behavior was reported for $[Mo^{IV}O(1,2\text{-}S_2\text{-}3\text{-}Ph_3SiC_6H_3)_2]^{2-}$ with bulky substituents.[30] In these cases, the *trans*−*cis* rearrangement of the intermediate is the rate-determining step. The sufficient bulkiness and/or NH···S hydrogen bonds stabilized the intermediates and retarded the rearrangements. In the present case, such a significant saturation behavior was not found. The hydrogen bond stabilized the intermediate moderately, and the insufficient bulkiness allowed a facile rearrangement. To reveal the relationship among the strength of the hydrogen bond, the bulkiness of the substituent group, the rate constant, and the reaction mechanism, further systematical investigations are required, which will be reported in the near future.

The reaction was also followed by ^{1}H NMR. When an equimolar mixture of *trans*/*cis* isomers was used, the two isomers reacted with Me_3NO to the same extent; that is, the 1:1 ratio was maintained during the reaction, as shown in Figure S5. The reaction was clean and afforded pure **2** as the only structural isomer accompanying the conversion of Me_3NO into Me_3N. These results suggest that the reactivities of the *trans*- and *cis*-isomers of **1** are identical.

Structural Characterization of Dioxomolybdenum(VI) Complex. The purity of isolated **2** was confirmed by ^{1}H NMR, where neither unreacted Me_3NO nor product Me_3N could be found. The ^{1}H NMR spectrum of **2** in acetonitrile-d_3 for aromatic and *t*-Bu regions is shown in Figure 5 in comparison

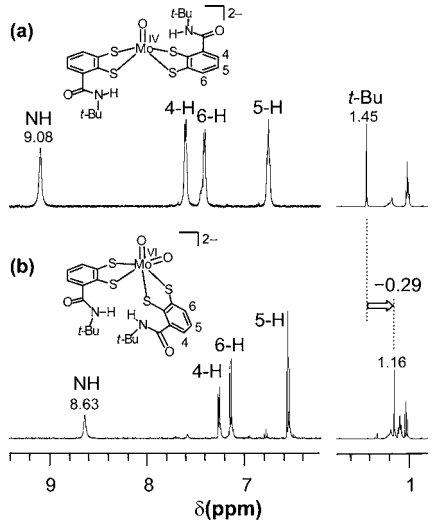

Figure 5. ^{1}H NMR spectra of (a) *trans*-$(NEt_4)[Mo^{IV}O(1,2\text{-}S_2\text{-}3\text{-}t\text{-}BuNHCOC_6H_3)_2]$ (*trans*-**1**), and (b) $(NEt_4)_2[Mo^{VI}O_2(1,2\text{-}S_2\text{-}3\text{-}t\text{-}BuNHCOC_6H_3)_2]$ (**2**) in acetonitrile-d_3 at 30 °C. The aromatic region was enlarged along vertical axis.

with **1**. As described in detail below, the peaks were fully assigned by HMBC, HSQC, GOESY, and NOESY spectra, and the assignments are shown with labeled chemical structures.

The ^{1}H−^{13}C HSQC correlation spectrum indicates directly bound ^{1}H−^{13}C (Figure S6b). The ^{1}H−^{13}C HMBC spectrum revealed multiple bond interactions, including single bonds (Figure S6a). To reduce the thermal motion and increase the sharpness of the signals, two-dimensional spectra were recorded at −10 °C. Consequently, we were able to make a reasonable assignment, as shown in Figure 5. A single set of proton signals for the ligand indicated the presence of a single symmetric isomer in the ^{1}H NMR time scale. When octahedral geometry is assumed and enantiomers are neglected, three isomers **2A**−**2C** are possible (Figure 6). In the case of the catecholate derivative of dioxomolybdenum(VI), *cis*-$(NMe_4)_2[Mo^{VI}O_2(2,3\text{-}dhb)_2]$ (2,3-H_2dhb = 2,3-dihydroxybenzoic acid),[38] which contains two intramolecular OH···O hydrogen bonds and similar octahedral geometry to **2**, two distinct isomers in a roughly 2:1 ratio were detected by ^{1}H NMR. The major isomer had symmetric coordination as ascertained by the single set of proton resonances of the ligand observed, where both hydrogen-bonded O^- ligands were *trans* to the oxo ligand like isomer **2A**. The minor isomer, like isomer **2C**, had unsymmetrical coordination as ascertained by the two sets of proton resonance with the same integral intensity observed. For complex **2**, either isomer **A** or **B** (Figure 6) was possible

dx.doi.org/10.1021/ic301597d | *Inorg. Chem.* 2012, 51, 11688−11697

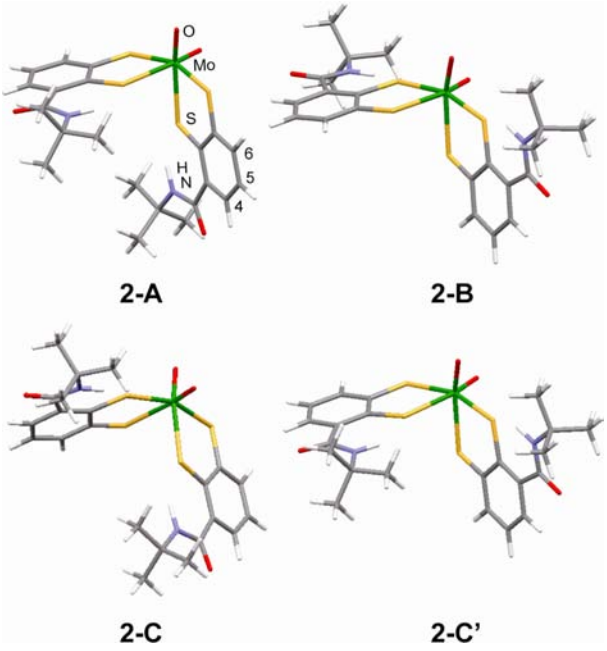

Figure 6. Structures of isomers **2A**–**2C** (**2C**′) of $[Mo^{VI}O_2(1,2\text{-}S_2\text{-}3\text{-}t\text{-}BuNHCOC_6H_3)_2]^{2-}$ obtained by DFT geometrical optimization. **2C** and **2C**′ are identical.

because of the observation of the single set of signals. The ^{1}H NMR signals of **2** were found upfield from those of **1** (Figure 5). The proton signal of the *t*-Bu group was observed at 1.16 ppm, which is upfield from that of **1** by 0.29 ppm. The NH signal of **2** was found at 8.63 ppm, which is upfield from that of **1** by 0.45 ppm, although IR spectra revealed that the NH···S hydrogen bond of **2** is stronger than or of comparable strength to that of **1**. These results suggest that the upfield shifts of these protons are attributable to shielding effects induced by the aromatic rings, that is, the *t*-Bu group is located over the neighboring benzene ring of the other ligand in isomer **2-A**. It seems reasonable to conclude that isomer **2-A** is the predominant structure in solution, although conformational thermal motion must be present.

^{1}H NMR spectra of **2** at −10 °C revealed sharp peaks because of the restricted thermal motion. To estimate the spatial distances, GOESY spectra were measured, which indicated the presence of *t*-Bu groups in close proximity to three aromatic protons (Figure S7). The NOE correlation between *t*-Bu and 4-H is most likely due to an intraligand interaction with 4–5 Å distance (Figure S8). Because the 5-H and 6-H protons are ≥7 Å apart from the *t*-Bu group, the NOE must arise from an interligand interaction within the **2-A** isomer. The two ligands of **2-B** are directly opposite each other, making it impossible to assay the NOE-observable distance between protons. For the thioester *N*-*tert*-butyl-2,3-di(pivaloylthio)benzamide, no NOE correlation was observed between the *t*-Bu group and 5,6-H protons under similar conditions. One of the ligands of **2-A** was found capable of approaching another ligand within ∼4 Å by thermal motion.

DISCUSSION

Contribution of the NH···S Hydrogen Bond to Mo—S Bond Length. To evaluate the influence of NH···S hydrogen bonds, DFT calculations were carried out using B3LYP. The initial structures of *trans*-**1**, *cis*-**1**, and **3** were constructed on the basis of the X-ray structures with some modifications. The optimized structures are shown in Figure S9, and selected parameters are summarized in Table S2. In the table, Wiberg bond index and the atom–atom overlap-weighted natural atomic orbital (NAO) bond orders are shown in order to estimate the covalency of the bond. The hydrogen-bonded sulfur is labeled as S1 bound to C1, and the second sulfur is labeled as S2. In **3**, S1 and S2 are identical. The formation of the NH···S hydrogen bond was confirmed by the attractive interaction between the NH proton and S, the bond order of which was calculated as a positive value. On the basis of the bond order, the strength of the NH···S hydrogen bonds in *trans*-**1** and *cis*-**1** are approximately the same. Introduction of an amide group or an NH···S hydrogen bond in **3** shortened the Mo—S bonds. These results are consistent with the X-ray structure of **1**. The relatively longer length of the Mo—S1 bond compared with Mo—S2 also agreed with the crystal structure. Slightly shorter distances and a larger bond order of the Mo═O bond in *trans*-**1** and *cis*-**1** than in **3** are consistent with the observed ν(Mo═O) values in the Raman spectra.

Contributions of the NH···S hydrogen bonds to the M—S bonds have been investigated systematically. In the case of tetrakis(arenethiolato)metal complexes or monooxomolybdenum tetrakis(arenethiolate), the hydrogen bonds shorten M—S bonds. This phenomenon was explained by antibonding M—S interactions in the HOMO being diminished by NH···S hydrogen bonds, resulting in the increase of M—S covalency.[32,34,39] For porphyrin complexes, the situation is different. Such antibonding M—S character is not involved in the HOMO, and thus, the hydrogen bond simply decreases the electron density on sulfur; that is, it lowers the basicity of the thiolate ligand. Consequently, M—S bonds were elongated.[33,40,41]

For the optimized structure of *trans*-**1**, the HOMO is represented in Figure S10. Because an essentially nonbonding interaction between Mo and S was found, the donation of S to Mo should be reduced by NH···S hydrogen bonds. The bond order was significantly decreased by the hydrogen bond, while the calculated Mo—S1 bond length of **1** was apparently not elongated in the comparison with **3**. In contrast, the bond order of Mo—S2 of **1** was higher than that of **3**. This indirect contribution of the carbamoyl group was most likely acting through the dithiolene moiety or aromatic ring via π-conjugation. Such influences propagating through the delocalization system suggest to us the importance of the dithiolene moiety and the unsymmetrically connected pterin ring to the stabilization and electronic fine-tuning of the metal center in molybdenum enzymes.

The unsymmetrical electronic structure of **1** probably does not affect directly the binding of Me_3NO to the molybdenum center. The NH···S hydrogen bonds delocalize the electron on the molybdenum center through the thiolate ligand, resulting in facile acceptance of electrons from Me_3NO. The unsymmetrical structure of the ligand provides enough space to rotate the ligand, which is required by the *trans*–*cis* rearrangement.

In comparison with **3**, the presence of the NH···S hydrogen bonds augments the natural charge of Mo atoms, although the coordinated atoms lose their negative charge. These results indicate that the negative charge is delocalized on the ligand. In particular, the carbamoyl group and the hydrogen bond support the charge electrostatically. The more positive charge on Mo agrees with the positive shift found in the cyclic voltammograms.

dx.doi.org/10.1021/ic301597d | *Inorg. Chem.* 2012, 51, 11688–11697

The oxidation potential is correlated to the relative energy level of HOMO in DFT calculations. The calculated energy levels of HOMOs are listed in Table S2. One-electron oxidation from Mo(IV) to Mo(V) is removal of one electron on HOMO, which is formed primarily from orbitals of Mo(d_{xy}) and dithiolene moieties (Figure S10). The energy levels of *trans*- and *cis*-isomers of **1** are approximately equal. The difference of the calculated energy levels between *trans*-**1** and **3** is 0.033 au (0.91 eV). That is to say, the electron on HOMO of **3** is more easily removable than that of **1** by 0.9 V. The observed redox potential of **3** is more negative (i.e., easily oxiziable) than that of **1** by 0.12 V. Although contributions of solvating medium, used basis sets, theoretical method, and electronic configuration should be considered, the tendency agreed with the observation.

Thermodynamic Stability of Isomers of 1 and 2. The major isomer in the crude product of **1** is the *trans* isomer, indicating that the *trans* form is kinetically favorable in the ligand-exchange reaction. When *trans*-**1** was heated for several hours, it was converted to a 1:1 mixture of *trans*-**1** and *cis*-**1**, indicating that these isomers possess essentially equal thermodynamic stability. DFT calculations clearly indicated their identical stability as well. The calculated total energy is given in Table S2. The difference was only ~0.2 kcal mol^{-1}, which is a very small value even if it was underestimated.

As described in the discussion regarding ^{1}H NMR spectra, **2-A** is a unique isomer in solution. Unfortunately, **2** did not crystallize, and therefore the molecular structure could not be determined by X-ray analysis. Its thermodynamic stability was evaluated by theoretical calculations. The total energy of **2-A** was calculated to be less than that of **2-B** by ~6.0 kcal mol^{-1} (Table S3). This difference is not as large but clearly demonstrates that **2-A** is the more stable isomer.

Stabilization of the Mo^{VI}=O Bond by NH···S Hydrogen Bonds via *Trans* Influence. The first example of a dioxomolybdenum(VI) bis(dithiolate), $(NEt_4)_2[Mo^{VI}O_2(bdt)_2]$ (**6**), exhibited an extraordinarily long Mo—S (thiolate) bond (~2.6 Å) *trans* to the oxo ligand,[11,12] which is comparable to the Mo—S (thioether)[42] or Mo—S (thioketone) bond.[43] This long Mo—S bond is caused by strong donation of the oxo ligand at the *trans* position via *trans* influence,[12] and is stabilized by the adjacent dithiolene or aromatic ring to form a dithioketone-like contributing structure, closely related to the noninnocent behavior of the ligand. Conversely, a weak Mo—S bond stabilizes the M=O bond at the *trans* position.

Contributions of NH···S hydrogen bonds were evaluated by DFT calculations in both isomers **2-A** and **2-B** (Figure S9, Table S3). The bond order of NH···S revealed the presence of a hydrogen bond with covalent character, as well as the greater strength of the hydrogen bond of **2-A** over that of **2-B**. The Mo=O bond of **2-A** was significantly shorter than that of **6**, which is consistent with the Raman spectra. In addition, the Mo—S bond *trans* to Mo=O in **2-A** is longer than that of **6**. On the contrary, the hydrogen bond at the *cis* position of **2-B** elongated the Mo=O bond and shortened the Mo—S1 bond. These results demonstrate that the NH···S hydrogen bond stabilized the long M—S bond and strengthened the Mo=O bond at the *trans* position.

Furthermore, the hydrogen bond reduced the strained thioketone structure. The calculated distances of the S—C bonds are listed in Table S3. Relatively mild shortening of S1—C1 was found in **2-A** in comparison with **6**. Distribution of the natural charge clearly indicates the lopsided dithiolate ligand, where negative charge is localized on S1 in **2-A**. Such an unsymmetrical structure is usually unstable; however, the effective and selective NH···S hydrogen bonding stabilizes the localized negative charge and lowers the total energy.

Contribution of the NH···S hydrogen bond to the *trans* influence is illustrated in Figure 7. As described above, strong

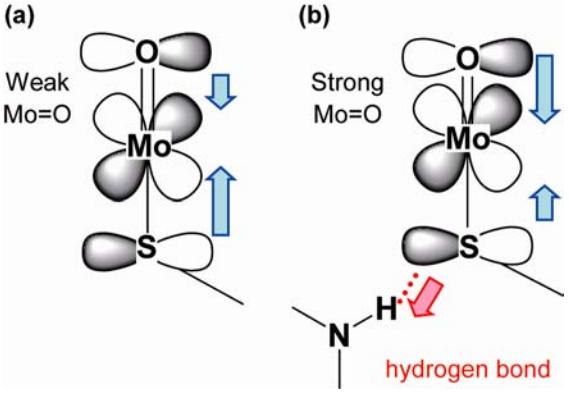

Figure 7. Schematic drawing of *trans* influence (a) without and (b) with NH···S hydrogen bond. The arrows represent the direction and degree of electron donation.

donation of S to Mo restricts the donation of O by *trans* influence, resulting in a weak Mo=O bond (Figure 7a). When an NH···S hydrogen bond is formed to the coordinated sulfur, electrons on the sulfur atom are used for the hydrogen bond, and thus, the donation from S to Mo is diminished. Consequently, the electron-deficient Mo requires electrons from the oxo ligand, which results in the strengthening of the Mo=O bond.

CONCLUSIONS

Monooxomolybdenum(IV) and dioxomolybdenum(VI) complexes with two intramolecular NH···S hydrogen bonds were successfully synthesized. Unsymmetrical introduction of an NH···S hydrogen bond into the benzenedithiolato ligand created an unsymmetrical coordination environment surrounding the molybdenum core. Two distinct Mo—S lengths were observed. The hydrogen bond stabilized and maintained the long Mo—S bond by moving the excessive electrons on the basic thiolate anion to the acidic NH. The dithiolene moiety most likely stabilized the local negative charge on the sulfur through the conjugated system that extended over the dithiolene and metal ion, which is known as noninnocent behavior. The dioxomolybdenum(VI) existed as a single isomer where Mo=O was *trans* to the hydrogen-bonded thiolato ligand, even though at least three isomers were possible. This selectivity indicates that the Mo^{VI}=O bond was effectively stabilized by the NH···S hydrogen bond via *trans* influence. These results suggest that the unsymmetrical coordination environment and conjugation system induced by the pterin cofactor are essential to regulating the activity of the molybdoenzymes, and that the NH···S hydrogen bonds most likely play a key role in the fine control of the reactivity of the active site.

In the present Article, unsymmetrical structure within one ligand was described; however, the two ligands are identical in a complex except for the reaction intermediates. In the active sites of DMSO reductase and trimethylamine *N*-oxide

dx.doi.org/10.1021/ic301597d | *Inorg. Chem.* 2012, 51, 11688−11697

reductase, the situation is different from our system. Two molybdopterin (P-MGD and Q-MGD) moieties are not identical in both enzymes. The molybdenum coordination spheres of the two enzymes resemble each other, although they show significant differences in substrate specificity, redox potential, and reactivity. The investigations using X-ray structural analysis have already revealed the difference in hydrogen bonding network of the MGD molecules to polypeptide chain and the protein environment in the active sites, caused by the differences in the sequences.[44] Further investigations to construct the sophisticated system in the active sites, including many weak interactions and surrounding media, are required in model studies.

■ ASSOCIATED CONTENT

Ⓢ Supporting Information

X-ray crystallographic data for **1** and *N*-*tert*-butyl-2,3-di-(pivaloylthio)benzamide in CIF format; crystallographic data (Table S1); molecular structure (Figure S1); ESI-MS of **2** (Figure S2); Raman spectrum of **2** (Figure S3); cyclic voltammograms of **1** (Figre S4); ^{1}H NMR spectra of **1** and **2** (Figure S5); HMBC, HSQC, GOESY, NOESY spectra of **2** (Figures S6–S8); optimized structures of model complexes (Figure S9); and geometrical parameters (Tables S2, S3), HOMO of *trans*-**1** (Figure S10). This material is available free of charge via the Internet at http://pubs.acs.org.

■ AUTHOR INFORMATION

Corresponding Author

*E-mail: tokamura@chem.sci.osaka-u.ac.jp.

Notes

The authors declare no competing financial interest.

■ ACKNOWLEDGMENTS

This work was supported by JSPS KAKENHI Grant 23655049.

■ REFERENCES

(1) Pushie, M. J.; George, G. N. *Coord. Chem. Rev.* **2011**, *255*, 1055–1084.
(2) Hille, R.; Nishino, T.; Bittner, F. *Coord. Chem. Rev.* **2011**, *255*, 1179–1205.
(3) Hill, R. *Chem. Rev.* **1996**, *96*, 2757–2816.
(4) Johnson, M. K.; Rees, D. C.; Adams, M. W. W. *Chem. Rev.* **1996**, *96*, 2917–2839.
(5) Holm, R. H.; Solomon, E. I.; Majumdar, A.; Tenderholt, A. *Coord. Chem. Rev.* **2011**, *255*, 993–1015.
(6) Enemark, J. H.; Cooney, J. J. A.; Wang, J.-J.; Holm, R. H. *Chem. Rev.* **2004**, *104*, 1174–1200.
(7) Smith, P. D.; Millar, A. J.; Young, C. G.; Ghosh, M.; Basu, P. *J. Am. Chem. Soc.* **2000**, *122*, 9298–9299.
(8) Ng, V. W. L.; Taylor, M. K.; Young, C. G. *Inorg. Chem.* **2012**, *51*, 3202–3211.
(9) Boyde, S.; Ellis, S. R.; Garner, C. D.; Clegg, W. *J. Chem. Soc., Chem. Commun.* **1986**, 1541–1543.
(10) Ueyama, N.; Yoshinaga, N.; Okamura, T.; Zaima, H.; Nakamura, A. *J. Mol. Catal.* **1991**, *64*, 247–256.
(11) Yoshinaga, N.; Ueyama, N.; Okamura, T.; Nakamura, A. *Chem. Lett.* **1990**, *19*, 1655–1656.
(12) Ueyama, N.; Oku, H.; Kondo, M.; Okamura, T.; Yoshinaga, N.; Nakamura, A. *Inorg. Chem.* **1996**, *35*, 643–650.
(13) Cowie, M.; Bennett. *Inorg. Chem* **1976**, *15*, 1584–1589.
(14) Baba, K.; Okamura, T.; Suzuki, C.; Yamamoto, H.; Yamamoto, T.; Ohama, M.; Ueyama, N. *Inorg. Chem.* **2006**, *45*, 884–901.
(15) Baba, K.; Okamura, T.; Yamamoto, H.; Yamamoto, T.; Ohama, M.; Ueyama, N. *Inorg. Chem.* **2006**, *45*, 8365–8371.
(16) Hsu, J. K.; Bonangelino, C. J.; Kaiwar, S. P.; Boggs, C. M.; Fettinger, J. C.; Pilato, R. S. *Inorg. Chem.* **1996**, *35*, 4743–4751.
(17) Davies, E. S.; Beddoes, R. L.; Collison, D.; Dinsmore, A.; Docrat, A.; Joule, J. A.; Wilson, C. R.; Garner, C. D. *J. Chem. Soc., Dalton Trans.* **1997**, 3985–3995.
(18) Matz, K. G.; Mtei, R. P.; Leung, D.; Burgmayer, S. J. N.; Kirk, M. L. *J. Am. Chem. Soc.* **2010**, *132*, 7830–7831.
(19) Matz, K. G.; Mtei, R. P.; Rothstein, R.; Kirk, M. L.; Burgmayer, S. J. N. *Inorg. Chem.* **2011**, *51*, 8904–9815.
(20) Sellmann, D.; Becker, T.; Knoch, F. *Chem. Ber.* **1996**, *129*, 509–519.
(21) Boyd, I. W.; Dabce, I. G.; Murray, K. S.; Wedd, A. G. *Aust. J. Chem.* **1978**, *31*, 279–284.
(22) Kondo, M.; Ueyama, N.; Fukuyama, K.; Nakamura, A. *Bull. Chem. Soc. Jpn.* **1993**, *66*, 1391–1396.
(23) Altomare, A.; Burla, M. C.; Camalli, M.; Cascarano, M.; Giacovazzo, C.; Guagliardi, A.; Polidori, G. *J. Appl. Crystallogr.* **1994**, *27*, 435.
(24) Sheldrick, G. M. *Acta Crystallogr.* **2008**, *A64*, 112–122.
(25) Frisch, M. J.; Trucks, G. W.; Schlegel, H. B.; Scuseria, G. E.; Robb, M. A.; Cheeseman, J. R.; Montgomery, J. A., Jr.; Vreven, T.; Kudin, K. N.; Burant, J. C.; Millam, J. M.; Iyengar, S. S.; Tomasi, J.; Barone, V.; Mennucci, B.; Cossi, M.; Scalmani, G.; Rega, N.; Petersson, G. A.; Nakatsuji, H.; Hada, M.; Ehara, M.; Toyota, K.; Fukuda, R.; Hasegawa, J.; Ishida, M.; Nakajima, T.; Honda, Y.; Kitao, O.; Nakai, H.; Klene, M.; Li, X.; Knox, J. E.; Hratchian, H. P.; Cross, J. B.; Adamo, C.; Jaramillo, J.; Gomperts, R.; Stratmann, R. E.; Yazyev, O.; Austin, A. J.; Cammi, R.; Pomelli, C.; Ochterski, J. W.; Ayala, P. Y.; Morokuma, K.; Voth, G. A.; Salvador, P.; Dannenberg, J. J.; Zakrzewski, V. G.; Dapprich, S.; Daniels, A. D.; Strain, M. C.; Farkas, O.; Malick, D. K.; Rabuck, A. D.; Raghavachari, K.; Foresman, J. B.; Ortiz, J. V.; Cui, Q.; Baboul, A. G.; Clifford, S.; Cioslowski, J.; Stefanov, B. B.; Liu, G.; Liashenko, A.; Piskorz, P.; Komaromi, I.; Martin, R. L.; Fox, D. J.; Keith, T.; Al-Laham, M. A.; Peng, C. Y. ; Nanayakkara, A.; Challacombe, M.; Gill, P. M. W.; Johnson, B.; Chen, W.; Wong, M. W.; Gonzalez, C.; Pople, J. A. *Gaussian03 (Revision E.01)*; Gaussian, Inc.: Pittsburgh PA, 2004.
(26) *Gaussian Basis Sets for Molecular Calculations*; Hujinaga, S., Ed.; Elsevier: Amsterdam, 1984.
(27) Yamanaka, S.; Kawamura, T.; Noro, T.; Yamaguchi, K. *J. Mol. Struct.* **1994**, *310*, 185–196.
(28) Zhu, X.; Yu, Q.; Greig, N. H.; Flippen-Anderson, J. L.; Brossi, A. *Heterocycles* **2003**, *59*, 115–128.
(29) Rosenfield, S. G.; Armstrong, W. H.; Mascharak, P. K. *Inorg. Chem.* **1986**, *25*, 3014–3018.
(30) Oku, H.; Ueyama, N.; Kondo, M.; Nakamura, A. *Inorg. Chem.* **1994**, *33*, 209–216.
(31) Kato, M.; Kojima, K.; Okamura, T..; Yamamoto, H.; Yamamura, T.; Ueyama, N. *Inorg. Chem.* **2005**, *44*, 4037–4044.
(32) Okamura, T.; Takamizawa, S.; Ueyama, N.; Nakamura, A. *Inorg. Chem.* **1998**, *37*, 18–28.
(33) Ueyama, N.; Nishikawa, N.; Yamada, Y.; Okamura, T.; Oka, S.; Sakurai, H.; Nakamura, A. *Inorg. Chem.* **1998**, *37*, 2415–2421.
(34) Ueyama, N.; Okamura, T.; Nakamura, A. *J. Am. Chem. Soc.* **1992**, *114*, 8129–8137.
(35) Oku, H.; Ueyama, N.; Nakamura, A. *Inorg. Chem.* **1995**, *34*, 3667–3676.
(36) Sugimoto, H.; Tarumizu, M.; Tanaka, K.; Miyake, H.; Tsukube, H. *Dalton Trans.* **2005**, *21*, 3558–3565.
(37) Ueyama, N.; Yamada, Y.; Okamura, T.; Kimura, S.; Nakamura, A. *Inorg. Chem.* **1996**, *35*, 6473–6484.
(38) Griffith, W. P.; Nogueira, H. I. S.; Parkin, B. C.; Sheppard, R. N.; White, A. J. P.; Williams, D. J. *J. Chem. Soc., Dalton Trans.* **1995**, 1775–1781.
(39) Ueyama, N.; Okamura, T.; Nakamura, A. *J. Chem.Soc., Chem. Commun.* **1992**, 1019–1020.
(40) Okamura, T.; Nishikawa, N.; Ueyama, N.; Nakamura, A. *Chem. Lett.* **1998**, *27*, 199–200.

(41) Ueyama, N.; Nishikawa, N.; Yamada, Y.; Okamura, T.; Nakamura, A. *J. Am. Chem. Soc.* **1996**, *118*, 12826−12827.
(42) Kaul, B. B.; Enemark, J. H.; Merbs, S. L.; Spence, J. T. *J. Am. Chem. Soc.* **1985**, *107*, 2885−2891.
(43) Berg, J. M.; Hodgson, K. O. *Inorg. Chem.* **1980**, *19*, 2180−2181.
(44) Czjzek, M.; Dos Santos, J. P.; Pommier, J.; Giordano, G.; Méjean, V.; Haser, R. *J. Mol. Biol.* **1998**, *284*, 435−447.